ISSN 0252-1075
Contribution from IITM
Research Report No. RR-109

Influence of El Nino on the Biennial and Annual Rossby Waves Propagation in the Indian Ocean with Special Emphasis on Indian Ocean Dipole

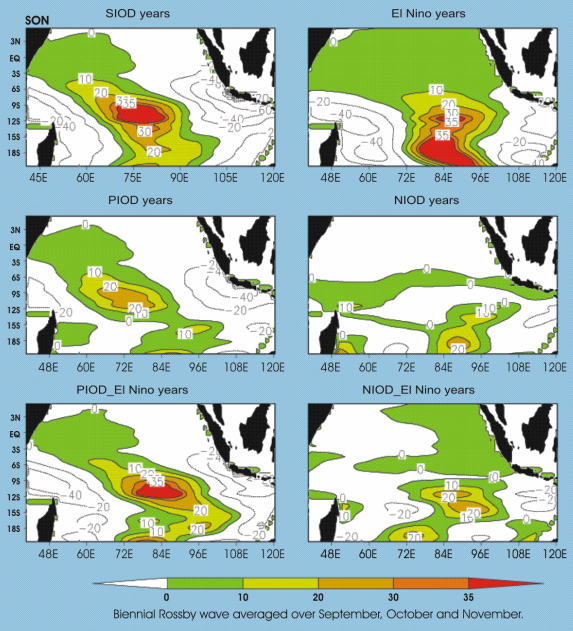

Biennial Rossby wave averaged over September, October and November.

B. H. Vaid, C. Gnanaseelan, P. S. Polito
and
P. S. Salvekar

January 2006

Indian Institute of Tropical Meteorology
Pune - 411 008, India

ISSN 0252-1075
Contribution from IITM
Research Report No. RR-109

Influence of El Nino on the Biennial and Annual Rossby Waves Propagation in the Indian Ocean with Special Emphasis on Indian Ocean Dipole

B. H. Vaid, C. Gnanaseelan, P. S. Polito
and
P. S. Salvekar

January 2006

Indian Institute of Tropical Meteorology
Dr. Homi Bhabha Road, Pashan Pune - 411 008
Maharashtra, India

E-mail : lip@tropmet.res.in Fax : 91-020-25893825
Web : http://www.tropmet.res.in Telephone : 91-020-25893600

CONTENTS

Influence of El Nino on the Biennial and Annual Rossby Waves Propagation in the Indian Ocean with Special Emphasis on Indian Ocean Dipole

B. H. Vaid, C. Gnanaseelan, P. S. Polito* and P. S. Salvekar

Abstract

The interannual variability of the tropical Indian Ocean is examined using 44 years (1958 – 2001) of Simple Ocean Data Assimilation (SODA) sea surface height anomalies and Hadley Centre Ice sea surface temperature (HADISST) anomalies. SODA sea surface height anomalies over the Indian Ocean is used to filter biennial and annual Rossby wave components using two-dimensional Finite Impulse Response filter. From the composite map of the biennial Rossby wave signals, a dipole pattern is clearly observed with the wave crest occupying the western Indian Ocean and the wave trough occupying the southeast tropical Indian Ocean during positive Indian Ocean dipole. Biennial Rossby wave signals play a significant role in strengthening the surface dipole in both western and eastern region of the tropical Indian Ocean. Downwelling biennial Rossby waves along 1.5^{o}S are seen propagating westward from the eastern boundary, more than one year prior to the formation of a positive Indian Ocean dipole. These strong downwelling signals are seen in the western equatorial Indian Ocean during the peak positive dipole time. The sea surface height in the western equatorial Indian Ocean is also controlled by the annual Rossby waves propagating from the eastern equatorial Indian Ocean. Further analysis demonstrates that biennial and annual Rossby waves are the major source of variability in the tropical Indian Ocean. Influence of El Nino on the propagation of biennial and annual Rossby waves in the Indian Ocean has been observed. In short, the present study supports the intrinsic link between Indian Ocean dipole and El Nino.

---

* Instituto Oceanográfico da Universidade de São Paulo (IOUSP), Brazil.

1. Introduction

The Indian Ocean Dipole (IOD) is a climate mode that occurs inter-annually in the tropical parts of the Indian Ocean. Normally it has been found that the sea surface temperature (SST) is low in the western Indian Ocean and high in the eastern Indian Ocean. But in some years this SST gradient reverses and causes shifting of convective activities over the western equatorial Indian Ocean, which is identified as IOD. A positive IOD is characterized by cool SST anomaly in the southeastern tropical Indian Ocean and warm SST anomaly in the western tropical Indian Ocean. Positive IOD years during the study period (1958 – 2001) are 1961, 1963, 1972, 1977, 1982, 1991, 1994 and 1997 (eight positive IOD years). Whereas a negative IOD is characterized by anomalously warm SST in the southeastern tropical Indian Ocean and anomalously cold SST in the western tropical Indian Ocean. Negative IOD years during the period are 1958, 1959, 1960, 1969, 1970, 1989, 1992 and 1996 (eight negative IOD years). The positive IOD events are associated with a decrease of sea surface height (SSH) in the eastern Indian Ocean and an increase in the western Indian Ocean. During a negative IOD the opposite pattern prevails. The see-saw pattern in the SSH anomaly during IOD is similar to the see-saw pattern in the thermocline. During several occasions both El Nino in the Pacific Ocean and IOD events in the Indian Ocean have co-occurred, but in many occasions IOD occurred during non El Nino years.

The development of IOD was associated with the propagation of Rossby waves in the tropical Indian Ocean [Vinayachandran et al., 1999; Gnanaseelan et al., 2005]. Rossby waves represent large scale dynamical response of the ocean to wind forcing and buoyancy forcing (heating and cooling) at the eastern boundaries and in the ocean interior. They can also be generated by perturbations along the eastern boundaries associated with coastal-trapped waves originating at lower latitudes. Murtugudde et al., [2000] and Gnanaseelan et al., [2005] suggested that the contribution of downwelling Rossby waves was crucial for sustaining the 1997 warming in the western Indian Ocean into February 1998. These studies have focused on documenting and analyzing the evolution of two most recent anomalous events in 1994 and 1997-1998. This preference is due to the reason that continuous observations of the oceanic heat content changes, such as the Topex/Poseidon altimeter measurements, became available in 1990's. In the present study, relatively longer time series data [1958 – 2001] has been taken into account to understand the propagation of Rossby waves in the Indian Ocean. Now it has been confirmed that understanding the mechanism of the interannual variability in the Indian Ocean, on

which predictability of the climate depends, is not possible without complete understanding of long equatorial waves (especially Rossby waves). The ocean dynamics suggest a certain amount of predictability to the IOD development once it has been triggered. However it is not clear until now what triggers IOD events, though there are various hypotheses suggesting different mechanisms [Annamalai et al., 2003; Gualdi et al., 2003 and Lau and Nath, 2004]. For instance, noting a strong correlation between IOD and ENSO events during boreal fall, some studies suggested that ENSO is a possible trigger for IOD events [Allan et al., 2001; Baquero-Bernal et al., 2002; Xie et al., 2002; Krishnamurthy and Kirtman, 2003; Annamalai et al., 2003]. However a number of strong IOD events have occurred in the absence of ENSO [Saji and Yamagata, 2003].

In this study role of biennial Rossby waves (BRWs) and annual Rossby waves (ARWs) in the IOD formation has been studied. Gnanaseelan et al., [2005] from relatively shorter time series of Topex/Poseidon altimetry data [during 1993 – 2001] found that anomalous downwelling BRWs along 1.5^{o}S, propagate westward from the eastern boundary in July/August of 1993 and 1996, about one year prior to the formation of positive IOD events. This strong downwelling signals reach the western equatorial Indian Ocean during the peak positive dipole time. These BRW signals are triggered by the wind stress curl in the eastern boundary, but are strengthened by the arrival of semi annual Kelvin waves. Since the analysis was based on relatively short period data, it is necessary to test this hypothesis using a longer time series. This issue is addressed in the present study by considering SSHA from SODA product for the period January/1958 to December/2001. Moreover the study investigates

- the nature and characteristics of BRWs and ARWs with special emphasis on wave generation, development and dissipation.
- the role of BRWs and ARWs in the formation of IOD.

The report has been organized as follows. In Section 2, a description of data and methodology is given. In Section 3, we focused results and discussion part. In section 3.1, we discuss the propagation of BRWs during the entire study period 1958 – 2001 with special emphasis on IOD. ARW's propagation is presented in section 3.2. IOD indices for HADISSTA, SODA SSHA and BRWs are explained in section 3.3. The results are summarized in section 4.

2. Data and methodology

The SSH data (from January/1958 – December/2001) derived from Simple Ocean Data Assimilation (SODA) product is used [Carton et al., 2000] in the analysis. Data region is $35^oE - 120^oE$, $30^oS - 20^oN$. The assimilation product used for SODA is based on Geophysical Fluid Dynamics Laboratory Modular Ocean Model 2.2. The Topex/Poseidon altimeter provides now more than a decade of sea surface height anomalies measurement with unprecedented accuracy of 2cm and the RMS (Root Mean Square) difference TOPEX/PESSODEN and SODA SSHA for 9 years (1993-2001) annual climatology is observed to be less than 1.2 cm (for area averaged grid points). The spatial map (for all the grid points) showed that RMS difference is high (more than 5 cm) over the Somali coast while in the most of the Indian Ocean difference is less than 3 cm. The Hadley Center Ice sea surface temperature (HADISST) Global Ocean Surface Temperature analysis [Rayner et al., 2003] was also used.

The two dimensional Finite Impulse Response (FIR) filter which is band pass filtering technique used to filter the SODA SSH anomalies into biennial and annual Rossby wave components. FIR filters are based on convolution of two sequences, the original data η_0 and the filter f, resulting in the filtered data η_f. In the present case $\eta_0(x,t)$, is a function of longitude and time, therefore the filter f(i,j) is a function of longitudinal lag i, and temporal lag j. The filtered matrix is given by,

$$\eta_f(x,t) = \sum_{i=-m}^{m}\sum_{j=-n}^{n}\eta_0(x+i,t+j)f(i,j), \qquad \text{(A)}$$

The size of the filter is controlled by the parameters m & n.

For band pass filtering of biennial and annual Rossby waves component, the filter f(i, j) is a Gaussian tapered cosinusoidal surface.

$$f(i,j) = \frac{e^{-\frac{1}{2}\left\{\left(\frac{\pi i}{m}\right)^2+\left(\frac{\pi j}{n}\right)^2\right\}}}{N}\cos\left(\frac{2\pi i}{L}-\frac{2\pi j}{T}\right)+M\,, \qquad \text{(B)}$$

with M and N such that

$$\sum_{i=-m}^{m}\sum_{j=-n}^{n}\left|f(i,j)\right| = 1,$$

$$\sum_{i}\sum_{j} f(i,j) = 0\,,$$

where L and T are the wavelength and period of the approximate centre of each pass band.

The FIR filter method offers an alternative, where each filter component covers a finite range of periods and wavelengths, a spectral band, instead of a spectral line. Amplitudes, periods and wavelengths can vary within certain thresholds, with the period chosen a priori, centered within the bandwidth. No functional shape is assumed and the data are processed simultaneously in the time and longitude domains. This makes the filter design process more intuitive thus easier to adapt to oceanographic applications in which two out of the three parameter cp, T and L are known to be within a certain range. The filter parameters are adjusted to bracket the spectral bands related to previously observed physical processes. This is an advantage to classical Fourier analysis and complex empirical orthogonal functions, since both methods do not allow for such adjustment. The details of FIR filter are given in Polito et al., 2000 and Polito et al., 2003.

Composite analyses have been carried out by taking filtered BRW and ARW components for the following cases:

a) Composite of 1961, 1994 and 1997, hereafter SIOD years [strong IOD years].
b) Composite of 1965, 1976 and 1986, hereafter El Nino years.
c) Composite of 1961, 1977 and 1994, hereafter PIOD years [positive IOD years].
d) Composite of 1972, 1982 and 1997, hereafter PIOD_El Nino years [positive IOD years coinciding with El Nino years].
e) Composite of 1959, 1970 and 1996, hereafter NIOD years [negative IOD years].
f) Composite of 1969 and 1992, hereafter NIOD_El Nino years [negative IOD years coinciding with El Nino years].

3. Results and Discussion

3.1 Biennial Rossby waves [BRWs] Propagation

Figure 1 shows the BRWs averaged over September, October and November [say SON] (a) SIOD years (b) PIOD years (c) PIOD_El Nino years (d) El Nino years (e) NIOD years (f) NIOD_El Nino years. Dipole like structure can be clearly seen in SIOD years, PIOD years and PIOD_El Nino years [Figure 1(a), 1(b) and 1(c)]. BRWs during SIOD years are observed to be stronger than the PIOD years and PIOD_El Nino years. Positive values indicate downwelling Rossby waves and negative values indicate upwelling Rossby waves. Downwelling BRWs were observed to be more dominant along 1.5^{o}S and 10.5^{o}S, which is consistent with the finding of Gnanaseelan et al., [2005]. A north-south oriented zero contour at about 85ºE separates the downwelling signals in the west and upwelling signals in the east. When the surface dipole attains its peak strength [SON], the downwelling BRW signals are more pronounced in the southern part of the tropical Indian Ocean (3ºS-10ºS, 60ºE-80ºE). Along with the downwelling signals in the west, upwelling BRW signals are also seen in the east during the dipole time, which gives a see-saw gradient in the SST. This is in agreement with the see-saw oscillation observed between the eastern and western equatorial HADISSTA in the Indian Ocean [Figure not shown]. So it is inferred that the BRW signals play a dominating role in strengthening the surface dipole in both western and eastern region of the tropical Indian Ocean. However, more detail study will be given in the forthcoming section. During El Nino years, NIOD years and NIOD_El Nino years, BRWs did not show any dipole like pattern [Figure 1(d), 1(e) and 1(f)].

Figure 2 shows BRW propagation along 1.5^{o}S during 1958 - 2001. Downwelling BRWs can be clearly seen propagating westward from the eastern boundary, about one year prior to the formation of the positive IOD events. This strong downwelling signals reach the western equatorial Indian Ocean during the peak phase of positive dipole. In normal years BRW signals propagate westward but do not reach up to the western boundary. More ever similar BRW propagation was observed in the subsurface also, which has been achieved by filtering BRW component from SODA heat content anomalies (125m depth) by FIR filter [Figure not shown]. However detail study is required to understand the processes accounting for its formation and developments. The FIR Filter reveals completely hidden dynamics along the equatorial Indian Ocean region in the form of BRW signals.

The behavior of BRWs was observed in all six different cases [as given in the Section 2]. Figure 3 shows BRWs signals at 1.5^{o}S (a) [0 indicates composite of 1960, 1993, and 1996, 1 indicates composite of 1961, 1994 and 1997, 2 indicates composite of 1962, 1995 and 1998], hereafter SIOD case. (b) [0 indicates composite of 1960, 1976, and 1993, 1 indicates composite of 1961, 1977 and 1994, 2 indicates composite of 1962, 1978 and 1995], hereafter PIOD case. (c) [0 indicates composite of 1971, 1981, and 1996, 1 indicates composite of 1972, 1982 and 1997, 2 indicates composite of 1973, 1983 and 1998], hereafter PIOD_El Nino case. In SIOD case, clearly BRWs started around July/August in the year preceding the SIOD years and reaches the western boundary by January/Feburary in the year following SIOD years [Figure 3(a)]. As the positive amplitude of the BRW reaches the western Indian Ocean by October/November, a pronounced increase in the SSH in the western Indian Ocean is seen [Figure not shown]. The comparison of PIOD case with SIOD case revealed that during PIOD case the wave propagation is weaker and started (reached) one month late (early) [Figure 3(b)].

During PIOD_El Nino case, BRW started around April/May preceding the PIOD_El Nino years and reached the western boundary March/April in the year following PIOD_El Nino [Figure 3(c)]. Similarly the BRW signals along 1.5^{o}S for (a) [0 indicates composite of 1964, 1975, and 1984, 1 indicates composite of 1965, 1976 and 1986, 2 indicates composite of 1966, 1977 and 1987], hereafter El Nino case. (b) [0 indicates composite of 1958, 1969, and 1995, 1 indicates composite of 1959, 1970 and 1996, 2 indicates composite of 1960, 1971 and 1997], hereafter NIOD case. (c) [0 indicates composite of 1968 and 1991, 1 indicates composite of 1969 and 1992, 2 indicates composite of 1970 and 1993], hereafter NIOD_El Nino case, were checked [Figure not shown]. BRW propagation was seen to be absent in El Nino case, NIOD case and NIOD_El Nino case, which further strengthen the findings of Gnanaseelan et al., [2005].

Even though the equatorial BRWs give insight into the coupled ocean atmospheric phenomena, another strong BRW signals are observed along 10.5^{o}S, we give a brief discussion on these BRWs and their propagation for all the six cases. Figure 4 shows composite of BRWs signals at 10.5^{o}S (a) SIOD case. (b) PIOD case (c) PIOD_El Nino case. During SIOD case, BRWs were seen to be starting from April/May of the preceding SIOD years and reaches the western boundary at 46^{o}E around November/December of the following SIOD years. In PIOD case, BRWs were seen propagating very slowly, it started one and a half years before the PIOD years and reached the western boundary at 48^{o}E around December next year. Now it is important to note that during PIOD_El Nino case, wave propagation started in

March/April and magnitudes were stronger than PIOD case. This infact supports the role of El Nino on BRWs, which will be further explored in the forthcoming discussion. Along 10.5^{o}S, BRWs were also seen in the El Nino case, but its origin was observed during October/November of the preceding months of El Nino years and it traveled with weaker intensity to reach the western coast. Moreover it reached the western boundary around October/November of the following years [Figure not shown]. No such propagation of BRWs was observed in NIOD case [Figure not shown], but during NIOD_El Nino case BRWs signal of 1 to 2cm were seen propagating around July/August of the preceding NIOD_El Nino years and reached western boundary at 48^{o}E around December of the following NIOD_El Nino years.

Above discussion suggests that the BRW propagates consistently throughout the entire study duration along 10.5°S, except NIOD case. But along 1.5^{o}S, BRWs propagation was seen only during SIOD years, PIOD years and PIOD_El Nino years.

Figure 5 shows the longitudinal plot of the BRW amplitudes for different time along different latitudes during SIOD years. Along 2.5°N, in SIOD years [Figure 5], the wave peak is centered at about 62°E during June and in the following months it intensifies. The peak reaches its maximum strength by November and is found at 55°E. Along 0.5°N, though the peak strength in November is very less but is located at 55°E. Along 2.5°S, the signal is seen similar to that of 2.5°N, and the peak of the BRW signal is maximum in November (~10mm). The wave peak along 5.5°S in the month of June is centered at 82°E. In November, maximum amplitude of wave was seen at 60°E. Along 8.5°S, the amplification at 70°E was not seen and the wave weakened from June to November. The wave amplitude maximum was located at 90°E (40mm) in June and after travelling westward reached 68°E by November with amplitude (30mm). Similar analysis has been carried out for PIOD years, PIOD_El Nino years, El Nino years, NIOD years and NIOD_El Nino years. It is observed that El Nino influence BRW on large extent in the south (maximum at about 12.5^{o}S), but its influence decreases as we move towards equator. In the equatorial Indian Ocean during October and November when the anomalous increase in SSH during the IOD period reaches its maximum strength, the BRW crest, lies between 55°E-65°E and thus contributing to the increase in SSH over this region.

Figure 6 shows the latitudinal plot of the BRWs amplitude for SIOD years. In SIOD years [Figure 6], during October/November at 90^{o}E trough of BRWs was seen

from 12°S – 4°S and crest of BRWs was seen from 3.5°S to 3.5°N. BRW crest from 3.5°S to 3.5°N was observed almost present at every longitudes. This confirms the existence of BRWs in the equatorial Indian Ocean between 3.5°S – 1.5°N as reported by Gnanaseelan et al., [2005]. BRWs propagation in this region starts with considerable amplitude but as it reaches or advances westward in the Indian Ocean its amplitude decay. At 70°E, 60°E and 55°E (during October/November) crest of BRWs is seen from 12°S – 4°S in almost all the months which confirms the role of BRWs in SST warming in this region. Amplitude of crest is also decayed as wave propagates westward. In PIOD years, BRWs propagation is more or less similar to SIOD years, but the magnitudes are weaker.

3.2 Annual Rossby waves [ARWs] Propagation

In this section detailed study of ARWs is carried out. Averaged over the latitudes 2.5°N, 4.5°N, 2.5°S, 3.5°S, 4.5°S, and 6.5°S is considered because ARWs mostly seen dominant at these latitudes [Gnanaseelan et al., 2005]. Figure 7 shows ARWs signals averaged over the above latitudes (a) SIOD case. (b) PIOD case (c) PIOD_El Nino case. In SIOD case, it can be clearly seen that ARW starts in the east during May/June and reaches the western Indian Ocean in February/March of the following years.

During PIOD case, ARWs were found to start one month earlier than SIOD case and is also weaker than SIOD case [Figure 7(b)]. It has been seen that during El Nino case wave propagation starts one month late as compared to SIOD case and the wave reaches the western Indian Ocean in April/May of the following years [Figure not shown]. Wave signals are stronger in SIOD case than in El Nino case. But during PIOD_ El Nino case, the temporal scale is more or less similar to El Nino case. It is noted that El Nino not only strengthen ARWs in the Indian Ocean but forms it about one month late (i.e., when there is El Nino in the Pacific Ocean, ARWs in the Indian Ocean start one month late). In NIOD case, weak ARWs propagation was seen. ARWs propagation starts in May and reaches the western Indian Ocean around October/November [Figure not shown]

From the above discussion it may be concluded that the SSH in the western equatorial Indian Ocean is also influenced by the ARWs propagating from the eastern equatorial Indian Ocean. In short, BRW signals and the ARW signals influence the evolution of the surface characteristics considerably during the IOD events.

Figure 8 shows the longitudinal plot of the ARW amplitudes for different time at different latitudes during SIOD years. In the SIOD years [Figure 8], maximum wave amplitudes were seen along 5.5°N in June around 50°E, and from then on its amplitude decreases in the subsequent months. But in November it strengthened again with a slight westward shift. Along 2.5°N the wave amplitude is maximum at 95°E in July and it is seen to travel westward in the following months with a decrease in the amplitude. By November the wave reaches 72°E and contributes to the increase in SSH, but the amplitude is very less (~12mm). In the southern hemisphere along 2.5°S, the wave starting at 100°E in June reaches 68°E by November and the amplitude up to 22mm i.e., higher than 2.5°N. Along 5.5°S the wave peak in June is around 88°E. In the subsequent months, as the wave propagates westward, its amplitude gets strengthened and reaches its peak strength in the month of October around 73^{o}E. By November, the wave peak lies at 70°E with amplitude of about 40mm and the positive amplitude extends from 55°E-80°E, thus contributing to the increase in the SSH in this region. Along 8.5°S the wave peak is amplified from June onwards till October and it moves from 95°E in June to 68°E in November. The maximum wave amplitude is 62mm. Along 12.5^{o}S, the wave propagated slowly and two wave peaks are present simultaneously in the ocean basin. In the month of November second peak has reached the western boundary and its amplitude is 35mm, where as first peak of high amplitude during November of the order of 60mm. Thus the waves dissipate as they reach the western boundary. Similar analysis was carried out for PIOD years, El Nino years, PIOD_El Nino years, NIOD years and NIOD_El Nino years. It has been observed that El Nino years influence the formation and arrival time of ARW. Further lot of variability was observed in the propagation of the ARWs in all the six different cases. The variability is pronounced more in north of 10°S. It is seen that the annual wave started earlier during PIOD years compared to the El Nino years. During the peak phase of the IOD the ARW has its maximum amplitude located around 60°E-80°E in the southern hemisphere north of 10°S. Thus the anomalous increase in SSH in this region can be thought of as a result of ARW propagation.

Figure 9 shows the latitudinal plot of the ARW amplitudes for different time along different longitudes during SIOD years. Along 90°E, in SIOD years [Figure 9], wave trough can be clearly seen during September to November from 10°S-Equator. The wave trough can be seen along 80^{o}E during October and November. Along 70^{o}E, most of the time, the wave crest is prominent and seen from 10°S-Equator. Maximum peak occurred around October/November. Further at 70^{o}E, along 4.5^{o}N second wave crest was seen. At 60^{o}E, only during October and November wave crest was observed in the above region. So ARWs play an important role in the formation of see-saw

pattern in the SST gradient during the IOD time. Similar results were observed in the ARW analysis for PIOD years but ARWs were observed to be weaker as compared to SIOD years.

In the El Nino years, during October/November the weak trough in the ARWs was seen at 90^{o}E and 80^{o}E. In NIOD years at 90^{o}E, during October/November wave crest of small amplitude was seen from 8^{o}S – 2^{o}N. At 70^{o}E and 60^{o}E, during October/November wave trough was prominent in the region 10^{o}S – Equator.

3.3 Dipole Mode Indices (DMI)

Saji et al., [1999] characterized the interannual variability in the Indian Ocean using a simple dipole mode index, which is the difference of SST anomalies between the western equatorial Indian Ocean region (50^o – 70^{o}E, 10^{o}S-10^{o}N) and tropical southeastern Indian Ocean (90-110^{o}E, 10^{o}S- Equator). They found that this SST anomaly pattern represents an internal mode of the variability within the Indian Ocean because the simultaneous correlation coefficient between the dipole and NINO3 indices is not high. The NINO3 index is defined as the averaged SST anomalies in the equatorial Pacific within 5^{o}S-5^{o}N, 90^{o}W-150^{o}W. However, considering that the two phenomena seem to have similar timescale, there may be a strong connection between them [Krishnamurthi and Kirtman, 2001]. Figure 10 shows dipole mode index for (a) HADISST anomalies (b) SODA SSHA (c) BRWs. Dipole mode indices for HADISST anomalies and BRWs have been calculated based on Saji et al., [1999], and seem to be well comparable.

Now to explore further, the dipole mode indices for both HADISSTA and BRWs were calculated in different cases [as given in the Section 2]. Figure 11 shows composite dipole mode index for HADISSTA (a) SIOD years (b) PIOD years (c) El Nino years (d) PIOD_El Nino years (e) NIOD years (f) NIOD El Nino years. Figure 12 shows composite dipole mode index for BRWs (a) SIOD years (b) PIOD years (c) El Nino years (d) PIOD_El Nino years (e) NIOD years (f) NIOD El Nino years. On comparing Figure 11 and 12, it can be said that BRW signals are observed to be comparable with HADISSTA for the different cases. This further strengthens the role of BRWs in the contribution of IOD.

4. Summary

This study investigates the behavior of westward propagating SSH anomalies across the tropical Indian Ocean, with a focus on the BRWs and ARWs (signals) filtered from SODA SSHA. These wave propagations have been examined in previous studies but a detailed study of this kind with a longer time series is very much required for understanding the dynamics and features during the different cases considered in the study. The FIR filter brought out these Rossby wave patterns from the SSHA data for entire period. From the composite maps of BRW, dipole patterns are clearly observed with the wave crest occupying the entire western Indian Ocean and the wave trough occupying the entire eastern Indian Ocean during the IOD peak phase. The BRWs are seen to propagate consistently throughout the year along 10.5°S, for all the cases except NIOD case. But along 1.5^{o}S, BRWs propagation was seen only during SIOD years, PIOD years and PIOD_El Nino years, which may be considered as the test of the hypothesis raised in Gnanaseelan et al., [2005].

In the equatorial Indian Ocean during October and November when the anomalous increase in SSH during the IOD period reached its maximum strength, the BRW crest, lies between 55°E-65°E thus contributing to the increase in SSH in this region. The SSH in the western equatorial Indian Ocean is also seen to be influenced by the ARWs propagating from the eastern equatorial Indian Ocean. Thus it is found that the BRW signals and the ARW signals control the evolution of the surface characteristics during the IOD events. From the propagation of BRWs and ARWs, it is evident that El Nino strengthen the BRWs and ARWs in the Indian Ocean.

Acknowledgements

We thank Director, IITM for providing the infrastructure required for the study. The financial support was provided by Department of Ocean Development, Govt. of India through DOD - INDOMOD project. The authors are thankful to Simple Ocean Data Assimilation (SODA) product team and Topex/Poseidon team for data. The authors acknowledge Dr. D. Sengupta, for scientific discussions and B. Thompson, J. S. Chowdary and A. Dey for their help during the preparation of the report. We thank Dr. R. Krishnan for reviewing this report. His critical comments and suggestions helped to improve the manuscript considerably.

REFERENCES

Allan R, D. Chambers, W. Drosdowsky, H. Hendon, M. Latif, N. Nicholls, I. Smith, R. Stone, Y. Tourre, 2001. Is there an Indian Ocean dipole, and is it independent of the El Nino- Southern Oscillation? CLIVAR Exchanges 6: 18–22 model. J. Atmos. Sci. 52: 1875–1902.

Annamalai, H., J. Potemra, R. Murtugudde, and J.P. McCreary, 2003. Indian Ocean Zonal Mode: Its decadal modulation and links to the Pacific. J. Clim., 18, 302-319.

Baquero-Bernal, A., M. Latif, and S. Legutke, 2002. On dipole like variability of sea surface temperature in the tropical Indian Ocean. J. Clim., 15, 1358-1368.

Carton, J.A., G. Chepurin, X. Cao and B Giese, 2000. A Simple Ocean Data Assimilation analysis in the global upper ocean 1950-95. Part I: Methodology, J. Phys. Oceanogr, 30, 294-309.

Gnanaseelan, C., B.H. Vaid, P.S. Polito, and P.S. Salvekar, 2005. Interannual variability of Rossby waves in the Indian Ocean & its impact on Indian Ocean Dipole, resubmitted to J. Geophys. Res., (JGR-Oceans).

Gualdi, S., E. Guilyardi, A. Navarra, S. Masina, and P. Delecluse, 2003. The interannual variability in the tropical Indian Ocean as simulated by a CGCM. Clim. Dyn., 20, 567–582.

Krishnamurthy, V., and B.P. Kirtman, 2001. Variability of the Indian Ocean: Relation to monsoon and ENSO. COLA Rep. 107, 39 pp.

Krishnamurthy, V., and B. Kirtman, 2003. Variability of the Indian Ocean: Relation to monsoon and ENSO. Q. J. R. Meteorol. Soc., 129, 1623–1646.

Lau, N.C., and M.J. Nath 2004. Coupled GCM simulation of atmosphere-ocean variability associated with zonally asymmetric SST changes in the tropical Indian Ocean. J. Clim., 17, 245-265.

Murtugudde, R., J.P. McCreary, A.J. Busalacchis, 2000. A Oceanic processes associated with anomalous events in the Indian Ocean with relevance to 1997-1998. J. Geophys. Res, 105, 3295-3306.

Polito, P.S., O.T. Sato, and W.T. Liu, 2000. Characterization and validation of the heat storage variability from TOPEX/POSEIDON at four oceanographic sites, J Geophys. Res., Vol. 105, No. C7, 16911-16921.

Polito, P.S., and W.T. Liu, 2003. Global characterization of Rossby waves at several spectral bands, J Geophys. Res., Vol. 108, No. C1, 3018, doi: 10.1029/ 2000JC000607.

Rayner N.A., D.E. Parker, E. B. Horton, C. K. Folland, L.V. Alexander, D.P. Rowell, E.C. Kent, A. Kaplan, 2003. Global analyses of sea surface temperature, sea ice, and night marine air temperature since the late nineteenth century. Journal of Geophysical Research 108, D14, 4407, doi:10.1029/2002JD002670.

Saji, N.H., B.N., Goswami, P.N. Vinayachandran & T. Yamagata, 1999. A dipole mode in the tropical Indian Ocean, Nature, 401, 360-363.

Saji, N., and T. Yamagata, 2003. Structure of SST and surface wind variability during Indian Ocean Dipole mode events: Coads observations. J. Clim., 16, 2735–2751.

Vinayachandran, P.N., N.H. Saji, and T.Yamagata, 1999. Response of the equatorial Indian Ocean to an unusual wind event during 1994, Geophys. Res. Lett., 26, 1613-1616.

Xie, S.P., H. Annamalai, F.A. Schott, and J.P. McCreary, 2002. Structure and mechanisms of south Indian Ocean climate variability, J Clim., 15, 864–878.

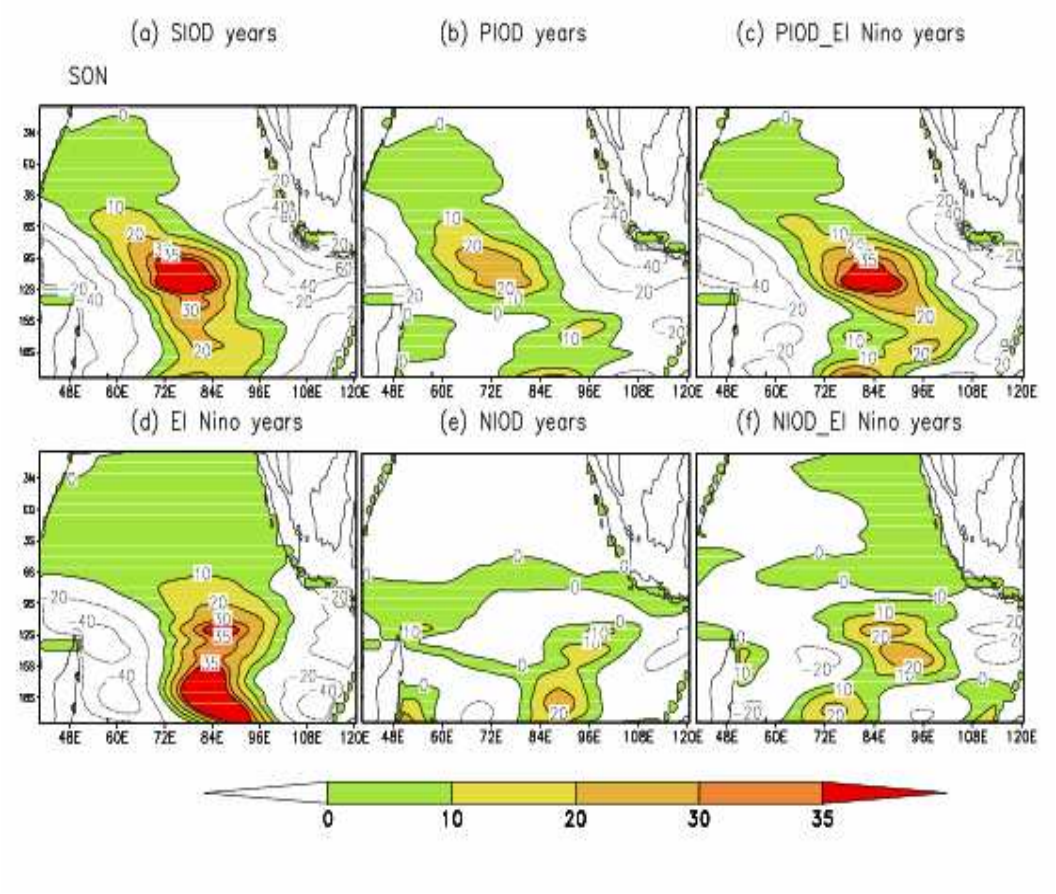

Figure 1: BRW averaged over September, October and November [say SON] (a) SIOD years (b) PIOD years (c) PIOD_El Nino years (d) El Nino years, (e) NIOD years (f) NIOD_El Nino years.

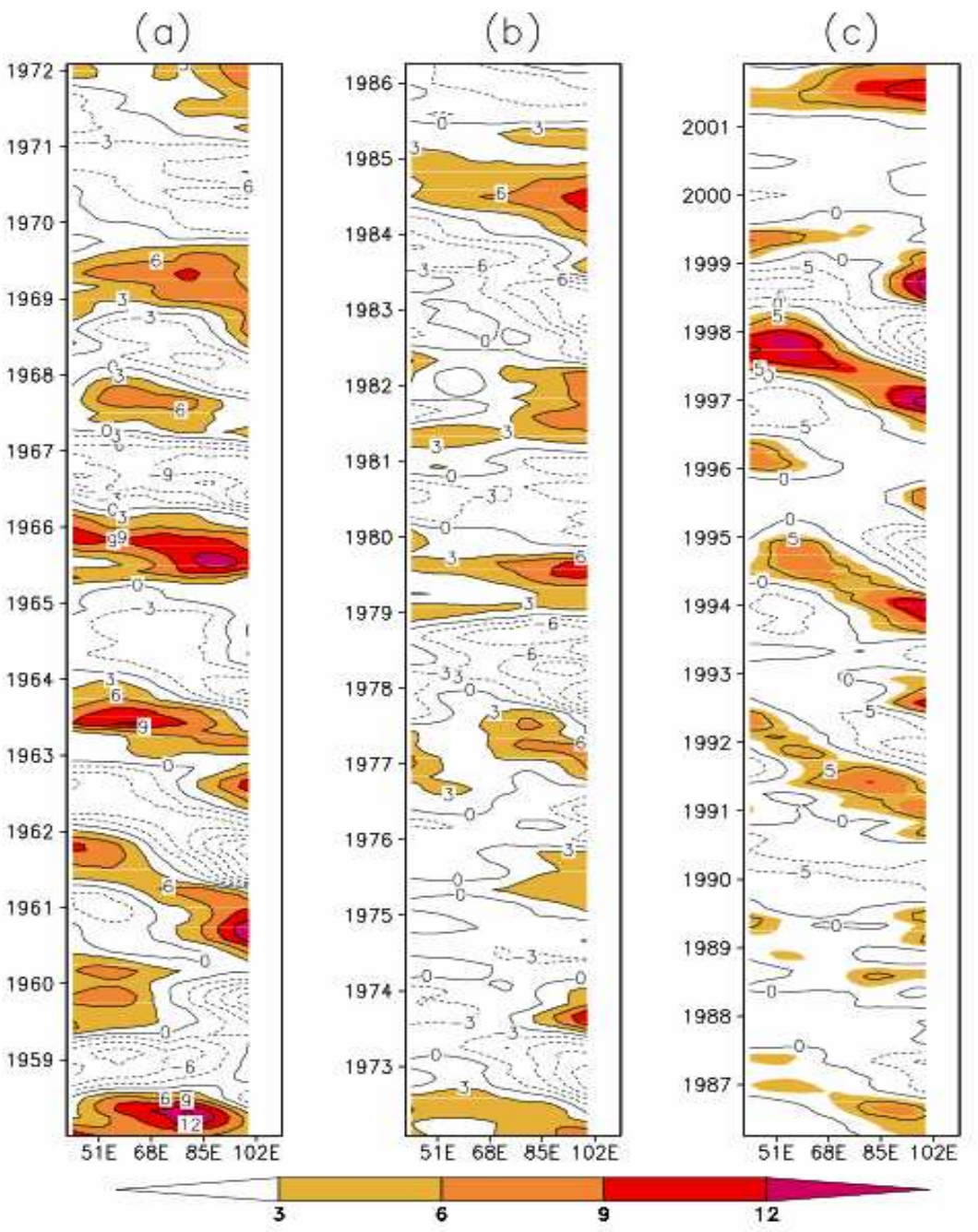

Figure 2: Propagation of BRW (mm) along 1.5°S.

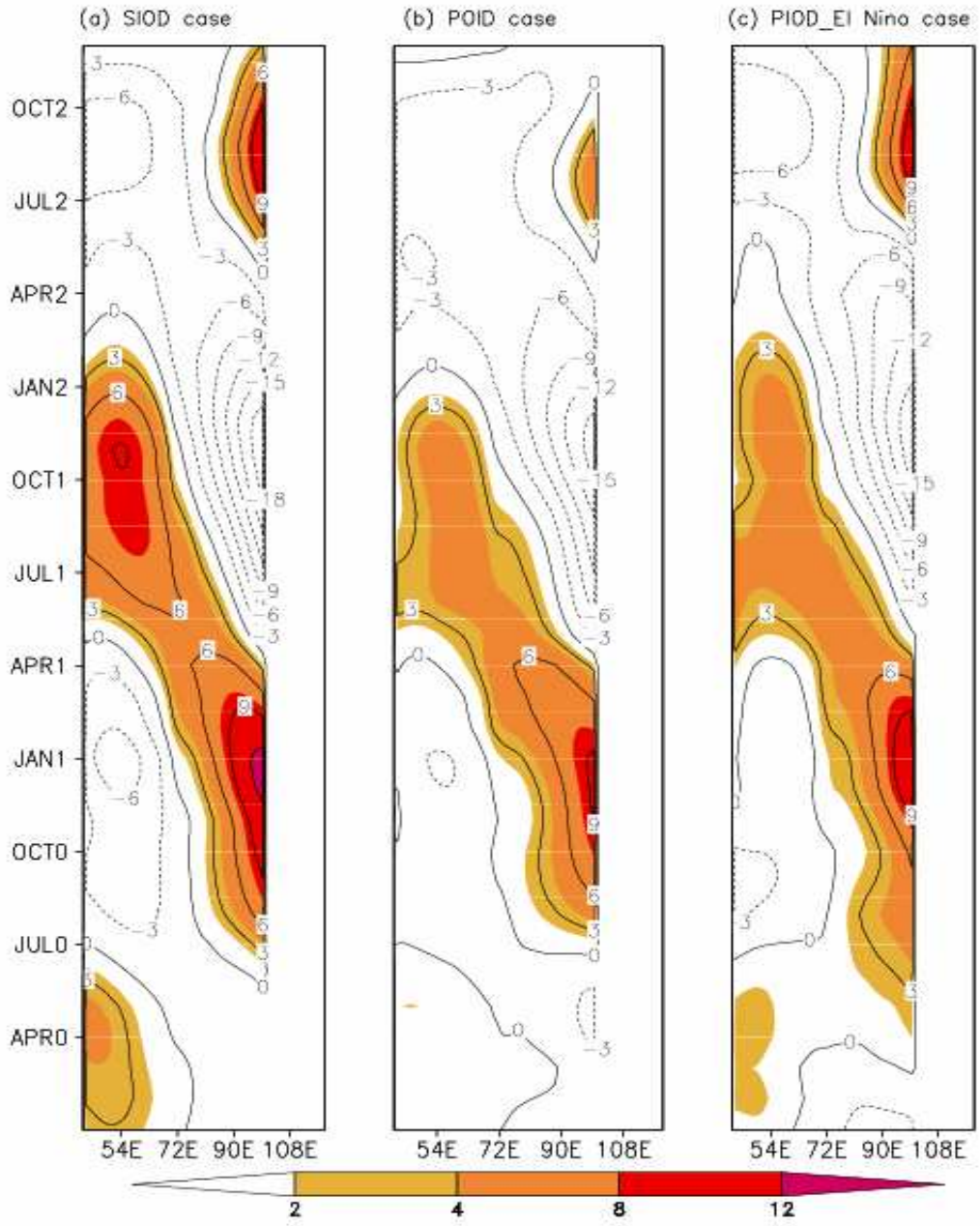

Figure 3: BRW signals along 1.5^{o}S (a) SIOD case. (b) PIOD case (c) PIOD_El Nino case.

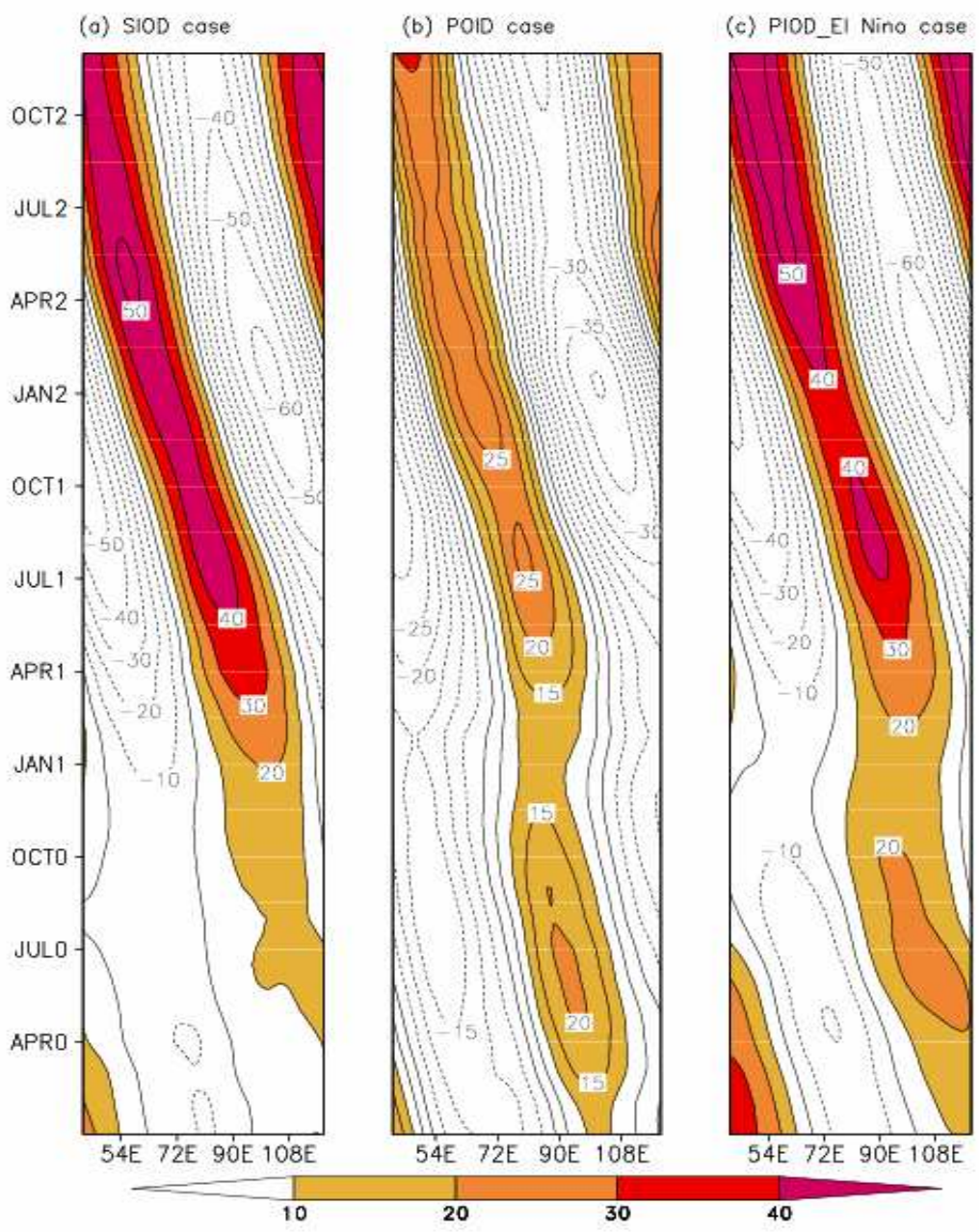

Figure 4: BRW signals along 10.5°S (a) SIOD case. (b) PIOD case (c) PIOD_El Nino case.

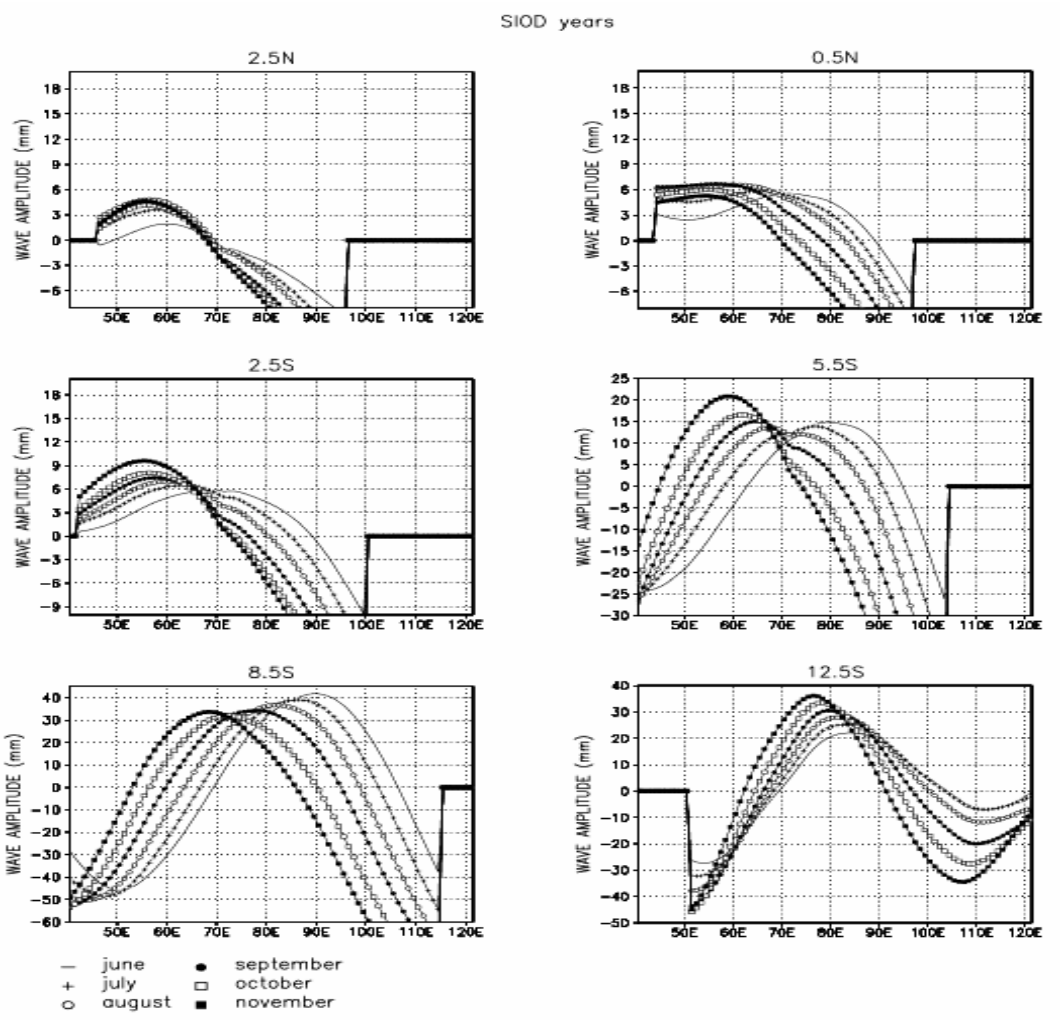

Figure 5: Longitudinal plot of BRW amplitude for different time at different latitudes during SIOD years.

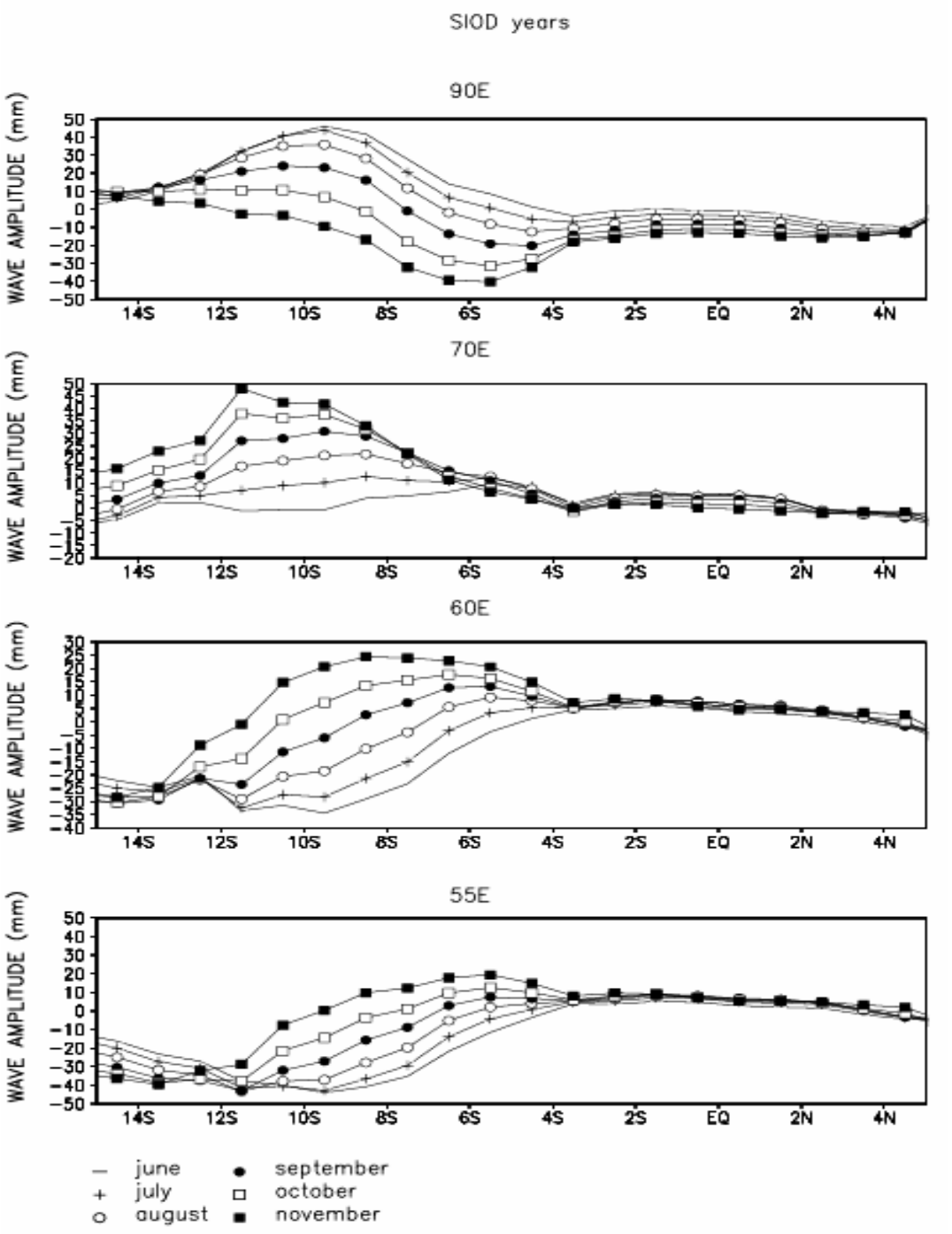

Figure 6: Latitudinal plot of BRW amplitude for different time at different longitudes during SIOD.

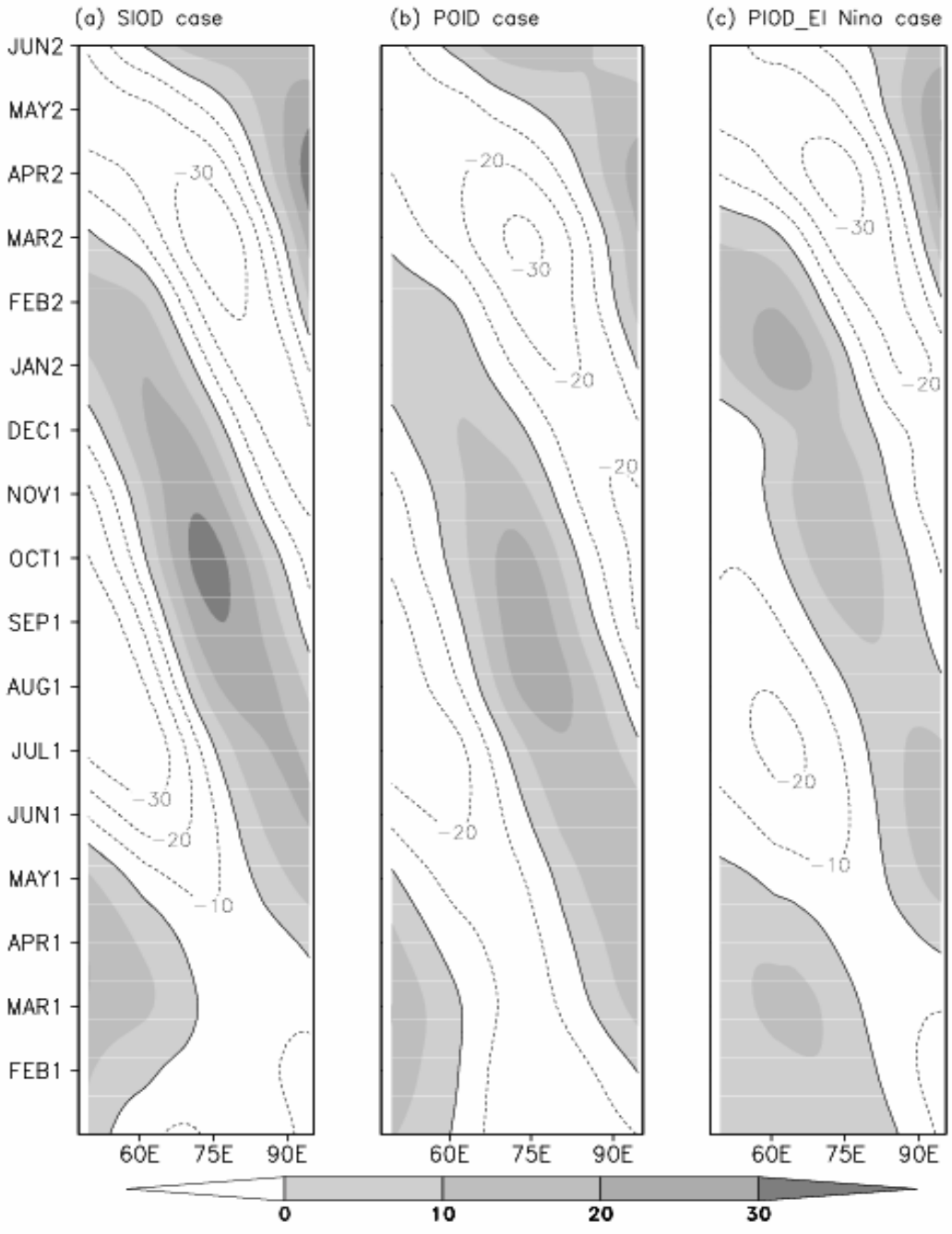

Figure 7: ARW signals averaged over 2.5°N, 4.5°N, 2.5°S, 3.5°S, 4.5°S, and 6.5°S (a) SIOD case. (b) PIOD case (c) PIOD_El Nino case.

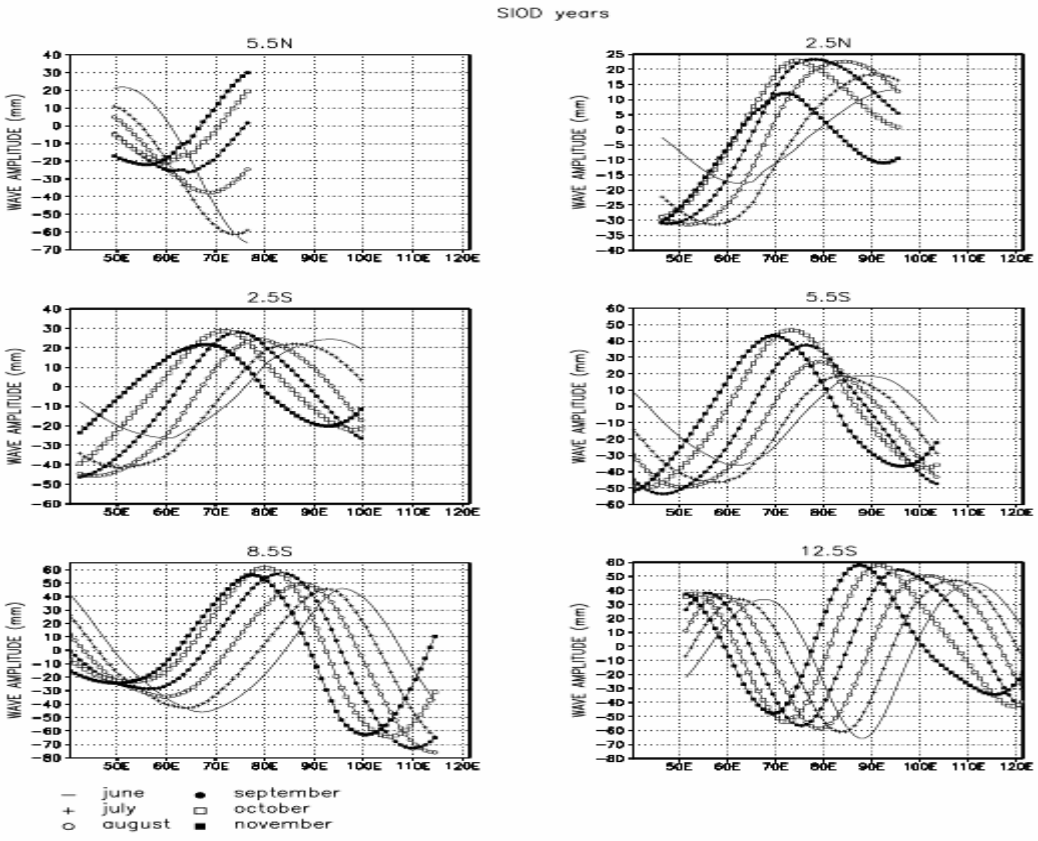

Figure 8: Longitudinal plot of ARW amplitude for different time at different latitudes during SIOD years.

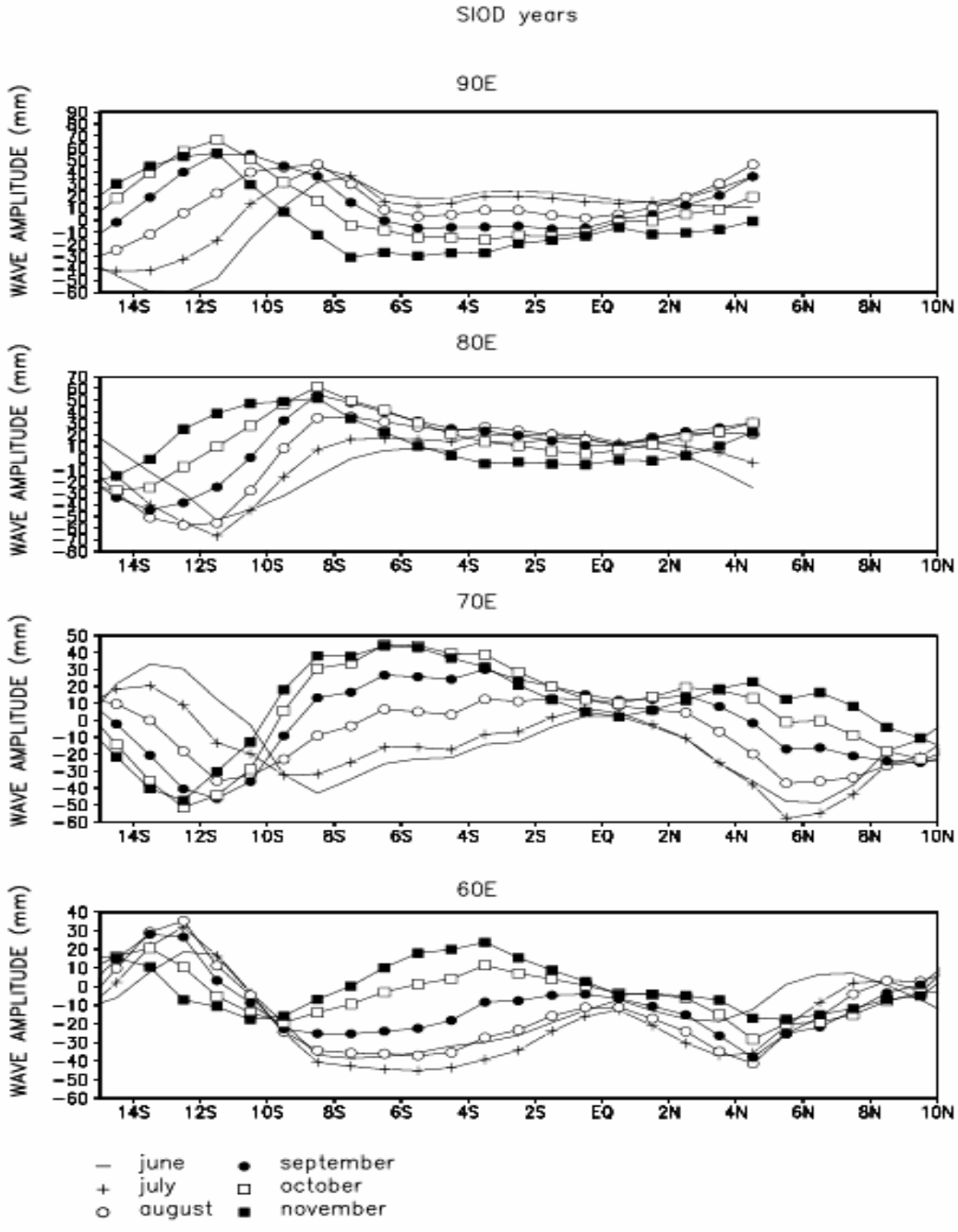

Figure 9: Latitudinal plot of ARW amplitude for different time at different longitudes during SIOD.

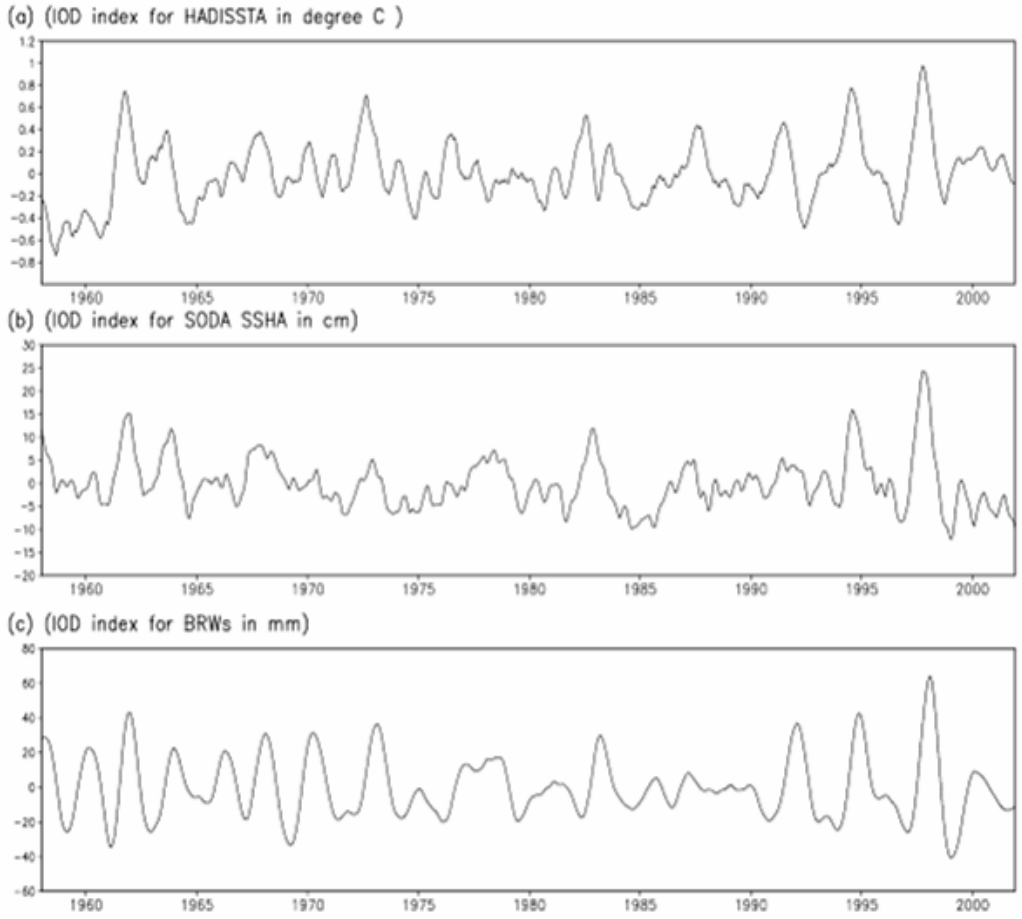

Figure 10: IOD indices for (a) HADISSTA [degree C] (b) SODA SSHA [in cm] (c) BRWs [in mm].

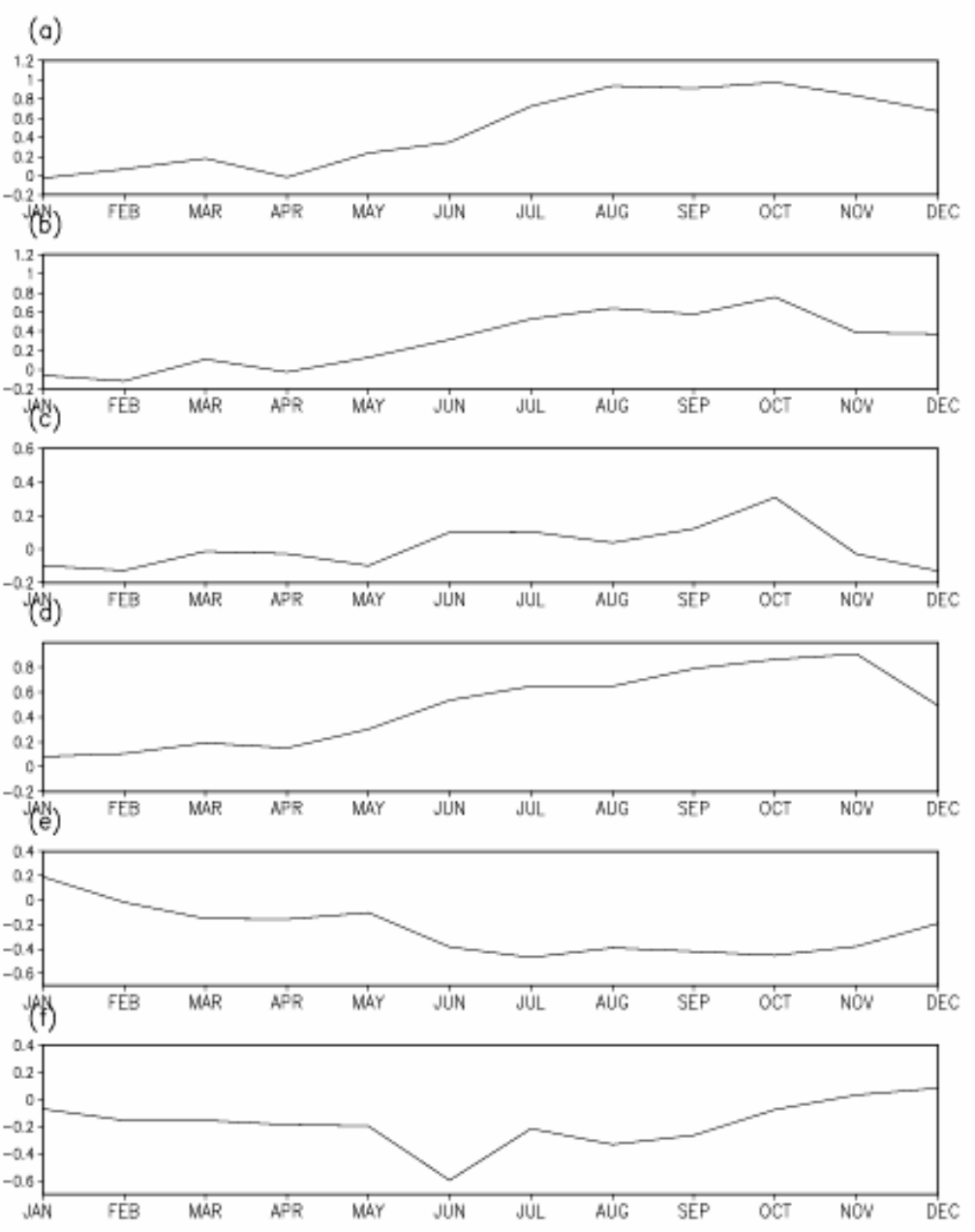

Figure 11: IOD indices for HADISSTA [degree C] (a) SIOD years (b) PIOD years (c) El Nino years (d) PIOD_El Nino years (e) NIOD years (f) NIOD_El Nino years.

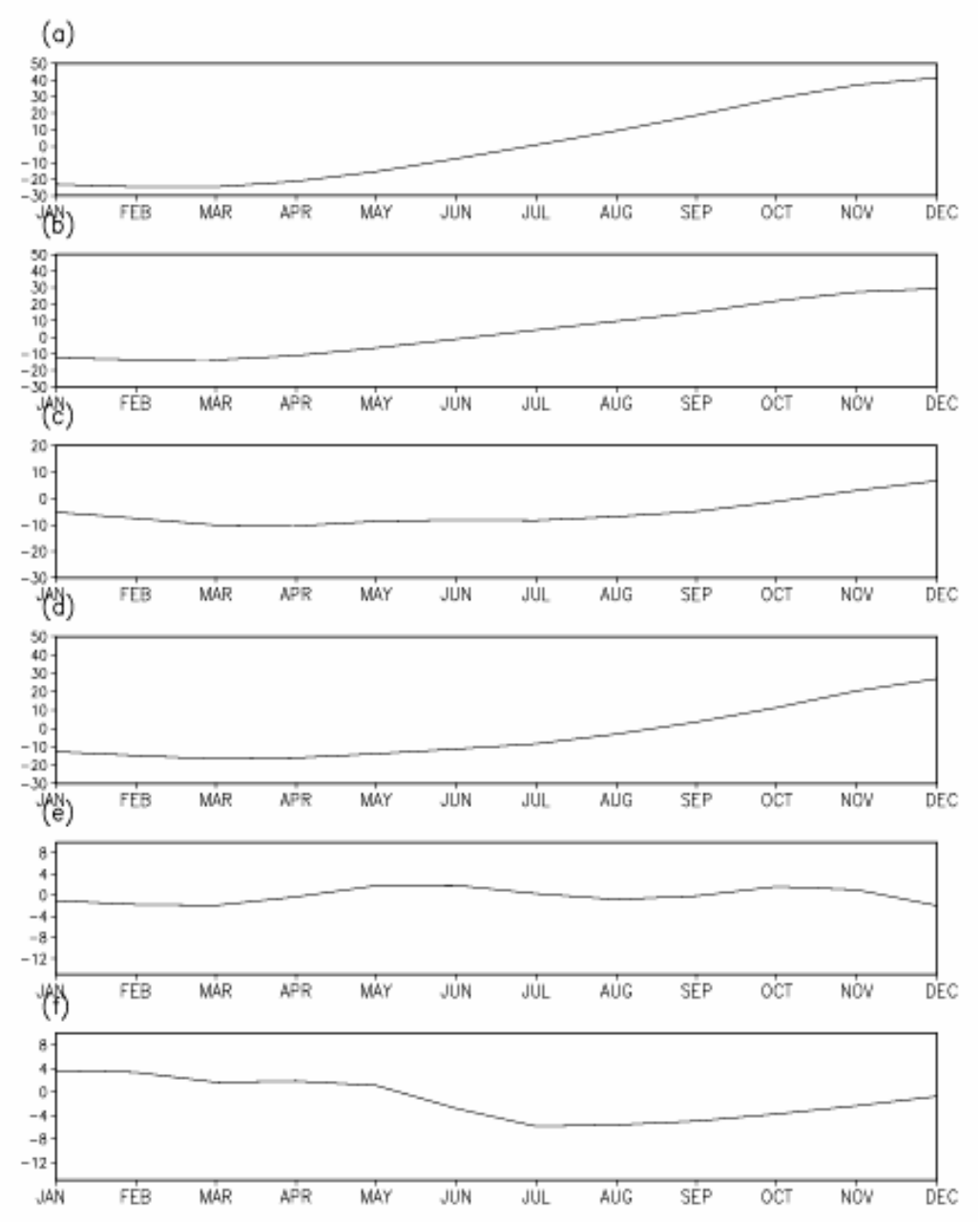

Figure 12: IOD indices for BRWs [mm] (a) SIOD years (b) PIOD years (c) El Nino years (d) PIOD_El Nino years (e) NIOD years (f) NIOD_El Nino years.